Metal-Micelle Interaction Leading to Spontaneous Formation of Ligand-Free Palladium(0) Nanoparticles: Highly-Efficient Catalysis Enabling Biaryl Ketones Formation from Carboxylic Acid Derivatives

Gaganpreet Kaur,[†] Jacek B. Jasinski,[‖] Fabrice Gallou,[§] Sachin Handa[†*]

[†]Department of Chemistry, University of Louisville, Louisville, Kentucky 40292, United States

[§]Chemical & Analytical Development, Novartis, 4056 Basel, Switzerland

[‖]Materials Characterization, Conn Center for Renewable Energy Research, University of Louisville, Louisville, KY, 40292, USA

KEYWORDS: micellar catalysis, chemistry in water, palladium nanoparticles, cross-couplings, amphiphile.

ABSTRACT: A novel strategy has been developed to spontaneously form ligand-free Pd(0) nanoparticles from water- and air-sensitive Pd_2dba_3 in water. These nanoparticles are thoroughly characterized by IR, NMR, and mass spectrometry, revealing that the metal-micelle binding plays a critical role in their stability and activity. HRTEM supported the ultrasmall nature of nanoparticles, while XPS analysis confirmed the zero-oxidation state of Pd. The shielding effect of micelles and enhanced stability of nanoparticles enabled fast cross-couplings of water-sensitive triazine adducts of carboxylic acid to form non-symmetrical biaryl ketones. These naturally formed nanoparticles are more efficient than new synthetic nanoparticles formed under a hydrogen atmosphere and traditional nanoparticles formed using air-sensitive Grignard reagent as a reductant. The activity of naturally formed nanoparticles is compared with synthetic nanoparticles over 34 substrates revealing that naturally formed nanoparticles are much more efficient than synthetic nanoparticles.

INTRODUCTION. Water is a natural and benign solvent with many exciting features to offer the best chemistry.[1-3] Upon adequate implementation, aqueous micellar catalysis can significantly reduce solvent consumption, waste generation, and energy usage.[4-8] The micellar hydrophobic interior may operate like protein's catalytic hydrophobic pockets, i.e., solubilizing the substrates to facilitate substrate-catalyst binding. The spontaneous formation of micelles above the critical micelle concentration is mainly an entropy-driven process minimizing the interface between hydrophobic molecules and water and, thus, reducing the system's free energy. In some instances, it can be both entropy- and enthalpy-driven phenomena.[9]

Nonetheless, following the same rule, when a metal salt is dissolved in the aqueous amphiphilic solution containing micelles, it could form nanoparticles (NPs). The dynamic nature of micelles and free amphiphilic molecules possessing suitable binding sites drive the spontaneous formation of NPs. These evolved NPs, in principle, can be more refined in size and catalytic efficiency compared to the ones synthetically formed. Furthermore, due to the binding nature of the amphiphile, the NPs formed via this method are phosphine ligand-free, and such ligand-free catalysts play a significant role in addressing sustainability challenges.[10,11] Notably, it is often wrongly perceived that the metal determines the cost of the catalytic method.[12] However, most of the time, the ligand adds to the cost and more waste, e.g., palladium (Pd) retains its identity after the catalytic process, although its oxidation state may change.[13] However, the ligand may not retain its original structure after the catalysis, or it may decompose. Therefore, ligand-free NP catalysis is more desirable.[8,14,15]

Compared to naturally evolved NPs, the synthetic Pd(0) NP's morphology, size, and the number of active sites largely depend on the nature of the reductant and solvents used in the synthetic procedure.[8,16] A careful selection of metal precursors is also a key to forming NPs.[17] Arylboronic acid has been used to obtain ligand-free Pd(0) NPs.[8] However, to the best of our knowledge, the detailed study of naturally formed Pd(0) NPs in aqueous micelles or traditional solvents is missing in the literature. Herein we report a systematic study of spontaneous and synthetic ligand-free NPs and their catalytic activities comparisons. We hypothesize that aqueous micelles of PS-750-M, due to the presence of tertiary amide units, can effectively bind with the metal atom to initiate nucleation for the spontaneous formation of Pd(0) NPs from their precursors (Scheme 1). Its shielding effect could further stabilize the air- and water-sensitive metal precursor, such as Pd_2dba_3.[18] For obtaining synthetic NPs from Pd_2dba_3, H_2 gas can be used as a reductant due to its higher solubility in aqueous micelles, causing de-ligation/reduction of dibenzylideneacetone (dba) readily. Because of metal-micelle binding, the resulting NPs can be catalytic and highly active for events needed for cross-coupling. Due to higher surface area of NPs and shielding effect of micelles, it is anticipated that the NPs as the catalyst should enable cross-couplings of water-sensitive intermediates, such as triazine adduct of carboxylic acids allowing ketones formation in water.

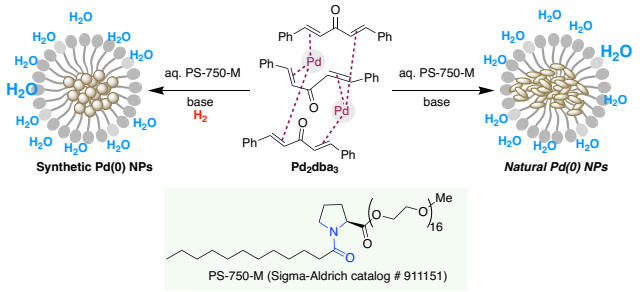

Scheme 1. Pd(0) nanoparticles (NPs) derived from Pd_2dba_3. Naturally formed NPs versus synthetic NPs formed under H_2 atmosphere.

RESULTS AND DISCUSSION. Following the proposed hypothesis, we obtained both the synthetic and natural Pd(0) NPs in aqueous micelles from Pd_2dba_3. Natural NPs were obtained by stirring Pd_2dba_3 in 3 wt % aqueous PS-750-M at basic pH (also see Supporting Information, page S2). In contrast, synthetic NPs were obtained by stirring Pd_2dba_3 in 3 wt % aqueous PS-750-M at basic pH and ambient hydrogen pressure. The *in-situ* reduction of one of the C=C bonds of dba in Pd_2dba_3 instantaneously free-up Pd(0) atoms for rapid nucleation to form NPs. Notably, no natural NP formation was observed in near water (see Figure S8 in the Supporting Information). The NPs obtained from both methods were analyzed by infrared (IR) and proton nuclear magnetic resonance (^{1}H NMR) spectroscopy for probing the interaction between Pd and the carbonyls of PS-750-M (Figure 1). The IR spectra of naturally formed (also called **NPs-1**) and synthetic NPs (also called **NPs-2**) are different, revealing that these two NPs most likely have different structures and bindings with amphiphile PS-750-M (Figure 1A). Likewise, **NPs-1** and **NPs-2** displayed different carbonyl stretches compared to free Pd_2dba_3 and PS-750-M, indicating the binding between PS-750-M and Pd via carbonyl functional groups. The carbonyls of neat PS-750-M appear at *ca*. 1630 cm^{-1}, while the same functional group in neat Pd_2dba_3 appears at 1638 cm^{-1}.

The control ^{1}H NMR studies also supports the binding between PS-750-M and Pd(0). The synthetic NPs displayed sharp signals at 7.30-7.18 ppm, most likely come from the aromatic rings of the reduced dba. The sharp signals are due to a lack of binding between reduced dba and NPs (Figure 1B). Reduction of dba under the hydrogen atmosphere and the subsequent de-ligation of the reduced ligand is confirmed by ^{1}H NMR spectroscopy and GC-MS analysis (see Supporting Information, pages S16-S17). Naturally formed NPs showed multiple broad signals between 7.17-6.07 ppm (Figure 1C). These signals showed upfield chemical shifts compared to the ones that appeared in the ^{1}H NMR spectrum of Pd_2dba_3 in aqueous PS-750-M (Figure 1D). This is due to the binding between PS-750-M with Pd present in the NP form that causes ligation between Pd(0) and dba through only one of the double bonds. The number of signals in the ^{1}H NMR spectra of Pd_2dba_3 and dba in D_2O/THF solvent also differed from the ones observed in **NPs-1**, further supporting no complete de-ligation of dba and the metal-micelle binding (Figure 1E, F). Thus, the control NMR studies support the binding between PS-750-M and Pd(0). It reveals that the NPs formed under hydrogen and argon atmospheres are having different chemical environment.

Next, the metal-amphiphile binding was further probed by mass spectrometry (Figure 1G), i.e., matrix-assisted laser desorption/ionization-time of flight (MALDI-TOF). NMR studies indicated that both the PS-750-M and dba bind with the Pd. However, on the Pd surface, PS-750-M may bind more strongly than the dba. If it is true, only the mass of Pd+PS-750-M was anticipated in the MALDI-TOF analysis of **NPs-1**. As per our expectation, a fragment from M–dba (Pd+PS-750-M) at 1122 amu was observed in the analysis. The absence of dba mass and the presence of PS-750-M mass in the Pd system further support that PS-750-M binds and stabilizes the Pd NPs. Thus, all spectroscopic studies together support the binding between PS-750-M and Pd.

High-resolution transmission electron microscopy (HRTEM) and high-angle annular dark-field scanning transmission electron microscopy (STEM-HAADF) was employed to examine morphology and particle size distribution. Energy-dispersive X-ray spectroscopy (EDS) mapping allows for the determination of the chemical composition and X-ray photoelectron spectroscopy (XPS) for studying the Pd's oxidation state. These analyses mentioned above were performed for **NPs-1** and **NPs-2**. These NPs were also compared with the ones formed by the reduction of Pd_2dba_3 with MeMgBr (called **NP-3**). The HRTEM and STEM-HAADF analyses of **NPs-1** revealed the formation of smaller NPs with an average diameter of 3.8 nm (Figure 2, A1-C1 and D1). No clumping was seen in these NPs, most likely due to stabilization provided by both PS-750-M and dba. The NPs were well dispersed due to their small size and interaction with amphiphiles.

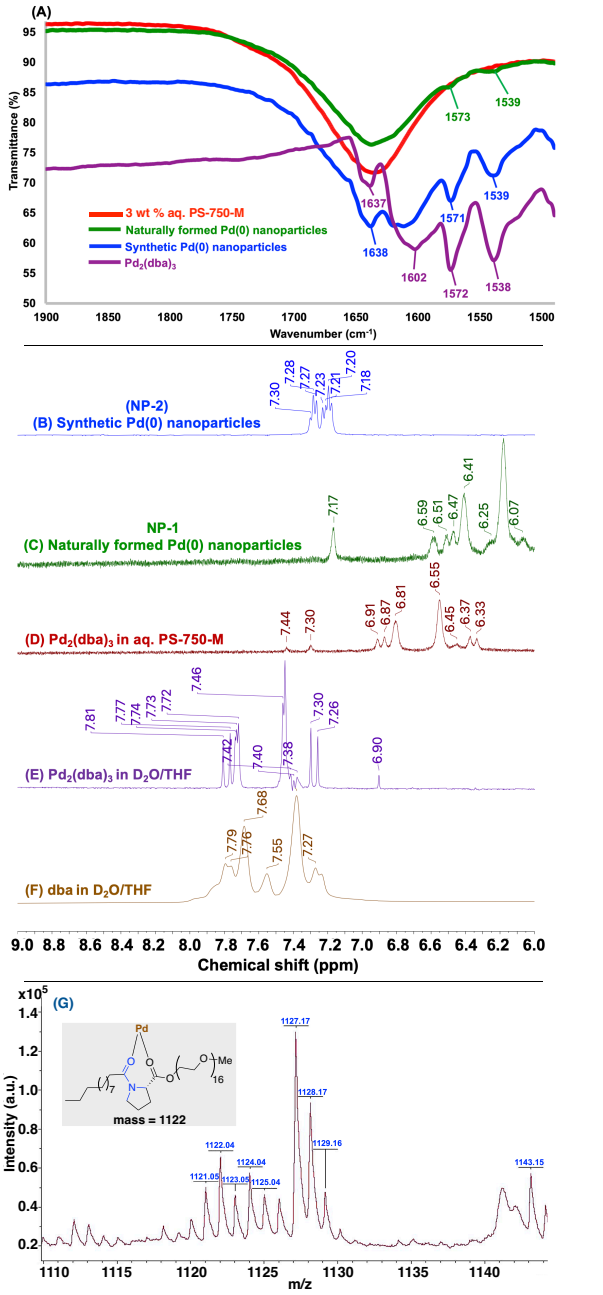

Figure 1. Detailed Characterization of synthetic and naturally formed nanoparticles. (A) Control IR study. (B-F) NMR studies revealing metal-micelle binding (H8-THF was used in the study). (G) MALDI-TOF of naturally formed nanoparticles supporting Pd-PS-750-M binding.

In contrast, **NPs-2** were larger (Figure 2, A2-C2) with an average diameter of 6.4 nm (Figure 2, D2). These NPs were dense and less uniformly dispersed, which may be due to fast nucleation and particle growth causing fast de-ligation of dba. However, NPs-3 were comparable to NPs-1, although some clumping was observed in them (Figures A3-C3). EDAX mapping of **NPs-1**, **NP-2**, and **NP-3** revealed the presence of Pd and carbon from PS-750-M (Figures E1, E2, E3). The low percent of the carbon in **NPs-2** was most likely indicative of a lesser number of amphiphiles per NPs compared to a more significant number of amphiphiles in **NPs-1** and **NPs-3**. Some clumping was also observed in **NPs-2**. XPS analysis of all NPs reveals the presence of Pd in a zero-oxidation state (Figures F1, F2, F3). However, more oxidized Pd was observed in **NPs-2** and **NPs-3**, which may be due to less or no shielding of NPs by micelles. The air exposure of NPs during analysis also causes their slight oxidation. Notably, the binding energy of Pd(0) in the peak deconvoluted spectra of Pd in **NPs-1 and NPs-3** was 334.9 eV. In comparison, it was 334.3 eV in **NPs-2**, revealing the different structures of metal-amphiphile binding in NPs.

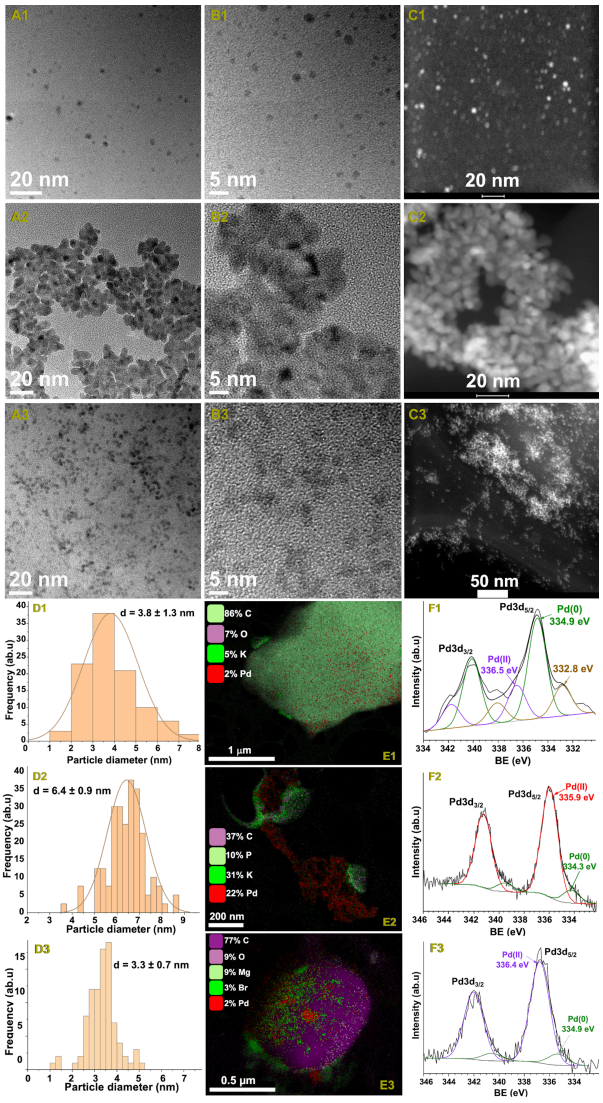

Figure 2. **Nanoparticles characterization.** (A1, B1) HRTEM analysis of **NPs-1**; (C1) STEM-HAADF analysis of **NPs-1**; (A2, B2) HRTEM analysis of the **NPs-2**; (C2) STEM-HAADF analysis of **NPs-2**; (A3, B3) HRTEM analysis of the **NPs-3**; (C3) STEM-HAADF analysis of **NPs-3**; (D1) histogram of **NPs-1**; (E1) EDAX analysis of **NP-1**; (F1) peak deconvoluted spectra of Pd in **NPs-1**; (D2) histogram of **NPs-2** (E2) EDAX analysis of **NP-2**; (F2) peak deconvoluted spectra of Pd in **NPs-2**; (D3) histogram of **NPs-3**; (E3) EDAX analysis of **NP-3**; (F3) peak deconvoluted spectra of Pd in **NPs-3**.

From detailed analytical studies, we found that these NPs contain Pd(0) atoms bound to PS-750-M, although **NPs-1** (naturally formed) were smaller in size and less oxidizable than **NPs-2 and NPs-3** (synthetic). Therefore, we decided to explore their catalytic activities on highly valued cross-couplings of water-sensitive triazine-acid adduct to access non-symmetrical biaryl ketones. Biaryl ketones have been recognized as one of the most critical structure motifs in pharmaceuticals,[19-22] natural products,[23] materials,[24] agrochemicals,[25] cosmetics,[26] and dyes.[27] Besides, such motifs are widely used as a synthetic intermediate for synthesizing various valuable compounds such as oximes,[27] cyanohydrins,[28] carbazones,[29] acetals,[30] and pinacols.[30] Their conventional or popular synthetic methods include: (i) Friedel-Craft acylation of arenes with a low regioselectivity, limited substrate scope, and requiring excessive Lewis acid.[29,30] (ii) Acylation of organometallic reagents requires anhydrous conditions and stoichiometric organometallic reagents and is incompatible with many functional groups.[31,32] (iii) Oxidation of secondary alcohols involving excessive strong oxidants.[33] Transition-metal catalyzed carbonylative couplings have also been reported for their synthesis.[34] However, such coupling methods involve highly toxic CO as the carbonyl source. Suzuki couplings of carboxylic acids via *in-situ* generated anhydride intermediate using different activating reagents have also been reported.[35,36] All these methods strictly require anhydrous conditions and toxic organic solvents.

Table 1. Optimization studies[a]

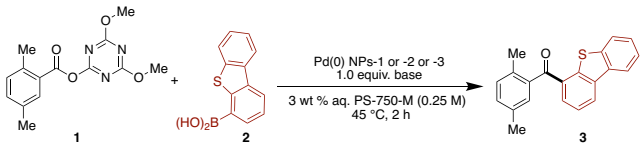

entry	Pd NPs and other conditions	**3** (%)[b]
1	1 mol % Pd NPs-1, [c]base K_3PO_4	51
2	2 mol % Pd NPs-1, [c]base K_3PO_4	55
3	3 mol % Pd NPs-1, [c]base K_3PO_4	72
4	3 mol % Pd NPs-1, base Et_3N	65
5	3 mol % Pd NPs-1, base K_2CO_3	82
6	3 mol % Pd NPs-1, base K_2CO_3, solvent THF instead of aq. PS-750-M	39
7	3 mol % Pd NPs-1, base K_2CO_3, solvent water instead of aq. PS-750-M	45
8	3 mol % Pd NPs-1, base K_2CO_3, reaction temperature 25 °C instead of 45 °C	56
9	3 mol % Pd NPs-2, [c]base K_3PO_4, reaction time 6 h instead of 2 h	52
10	4 mol % Pd NPs-2, [c]base K_3PO_4, reaction time 6 h instead of 2 h	64
11	4 mol % Pd NPs-2, [d]base K_3PO_4, reaction time 6 h instead of 2 h	56
12	no Pd NPs, [c]base K_3PO_4 or K_2CO_3	n.d.
13	3 mol % Pd NPs-3, base K_2CO_3	78

[a]**Conditions**: **1** (0.5 mmol), **2** (0.75 mmol), Pd **NPs-1** derived from $Pd_2(dba)_3$ or Pd **NPs-2** derived from $Pd_2(dba)_3$ and molecular hydrogen as reductant, base (0.5 mmol), 1.8 mL 3 wt % aq. PS-750-M, 0.2 mL THF, 45 °C, 2 h. [b]Isolated yield. [c]1.1 equivalent. [d]10 mol %.

We began our catalytic studies on carboxylation reaction in aqueous PS-750-M using carboxylic acid adduct **1** and boronic acid **2** as benchmark substate. Using 1 mol % *in-situ* formed Pd(0) **NPs-1** and K_3PO_4 as a base, 51% yield of **3** was obtained (Table 1, entry 1; for more details, see Supporting Information, page S21-S24). Notably, the reaction was completed in 2 hours. Therefore, we kept the reaction time 2 hours for the remaining optimization studies. Increasing the catalyst loading to 2 mol % did not significantly improve the yield (entry 2). 3 mol % catalyst afforded a 72% isolated yield of **3** (entry 3). However, 4 mol % catalyst loading did not improve the yield (see Supporting Information, Table S2, page S21). Therefore, we decided to use 3 mol % catalyst loading as optimal. Replacing K_3PO_4 base with Et_3N reduced the yield to 65% (entry 4), but K_2CO_3 base afforded an 82% isolated yield of **3** (entry 5). Therefore, we picked K_2CO_3 as an optimal base. PS-750-M was crucial for the catalytic activity. Reaction in neat THF affords only 39% product (entry 6), while in neat water, 45% of **3** was obtained (entry 7). Likewise, the reaction in toluene only affords 41% of **3** (Table S5, entry 2). Other surfactants, such as TPGS-750-M, SDS, Nok, SDC, and Pluronic, were not as effective as PS-750-M. However, Tween 20 provided 80% of **3** (Table S5, entries 4-10). This indicates that PS-750-M is crucial for Pd-micelle interaction as well as catalysis. Reducing the reaction temperature to 25 °C slowed the reaction rate, and only 56% of product **3** was obtained (entry 8). Thus, for **NP-1** as a catalyst, the optimal conditions were 3 mol % catalyst loading, 1.0 equivalent K_2CO_3 as a base, 45 °C reaction temperature, 0.25 global concentration, and THF additive (10 % relative to aq. PS-750-M; for more details of optimizations, see Supporting Information, pages S21-S24). Although **NPs-2** were easily oxidizable under air, these NPs worked also as catalysts under a non-oxidizable atmosphere. The *in-situ* generated **NPs-2** afforded a 52% isolated yield of **3** (entry 9). However, the reaction was completed in 6.5 h instead of 2 h. The slower reaction rate may be due to the larger NPs and lesser surface area of the catalyst. With the use of 1.1 equiv. K_3PO_4 as a base and higher catalyst loading (4 mol %), a 64% isolated yield of **3** was achieved in 6 hours (entry 10). The reaction also worked with the catalytic amount of K_3PO_4 (10 mol %), affording 56% of **3** (entry 11). Based on this initial activity test, **NP-2** were catalytically inferior to **NP-1**. No product **3** was obtained without a Pd catalyst (entry 12). Using K_2CO_3 base, **NPs-3** affords product **3** in 78% yield. (entry 13) However, these NPs were ineffective for other substrates, e.g., low yields of **21**, **22**, and **34** were obtained (see Supporting Information, page S32). Likewise, no reaction was observed when $Pd(dppf)Cl_2$ or $Ni(cod)_2/PCy_3$ were used as the catalyst (see Supporting Information, Table S9, page S24). $PdCl_2$/IPr catalyst afforded only 68% of **3**, revealing that **NP-1** acts as an efficient and sustainable catalyst. Due to the use of toxic Grignard reagents in their synthesis, inferior catalytic activity, and easily oxidizable nature, **NPs-3** were not selected for studying the full substrate scope.

The optimization studies showed that **NPs-1** and **NPs-2** are active, although reaction rates were slower with **NPs 2**. Therefore, we decided to perform a substrate scope using both kinds of NPs and compare their efficiency on a variety of substrates. In the substrate scope study, we used *in-situ*-formed NPs. To our delight, both NPs were active for cross-couplings of triazine adduct of carboxylic acids (Table 2, **3**-**37**). However, compared to **NPs-2**, reactions were generally completed faster with **NPs-1**. For example, for forming **3**, the reaction was completed in 2 hours with **NPs-1** and 6.5 hours with **NPs-2**, and the yield was significantly lower in the latter case. The couplings of adducts of heterocyclic carboxylic acids with heteroaryl boronic acid were amenable. Likewise, aromatic-aromatic and aromatic-heteroaromatic combinations worked well. Functional groups such as trifluoromethyl (**13**, **17**, **19**, **21**, **28**, **33**), Boc (**17**, **31**-**36**), aldehyde (**18**), and ester (**25**) were well tolerated. A combination of triazine adduct of thiophene carboxylic acid and thiopheneboronic acid afforded product **10** in excellent yield in only 2.5 hours. The adduct of pyridylcarboxylic acid (**29**) also worked well with the pyridylboronic acid. Boronic acids derived from benzothiophene (**6**, **22**, **34**), furan (**8**, **15**, **20**, **26**, **31**), pyridine (**5**, **14**, **23**, **27**, **29**, **37**), and thiophene (**4**, **10**, **25**, **32**) displayed good-to-excellent reactivity. Notably, reactions were generally fast and completed between 15 minutes to a few hours using **NPs-1**. Although reaction rates were slower with the use of **NP-2** catalyst, reaction yields were better in examples **5**, **9**, **17**, **19**, **21**, **24**, **27**-**29**, **33**, and **37**. Notably, the yields were significantly enhanced in example **33** when **NP-2** was used as the catalyst. Interestingly, under such a hydrogen environment and the presence of Pd, no Cbz cleavage was observed in example **37**. Notably, all carboxylic acid adducts were also synthesized in aq. PS-750-M (for details, see Supporting Information, page S20).

Table 2. Substrate scope[a]

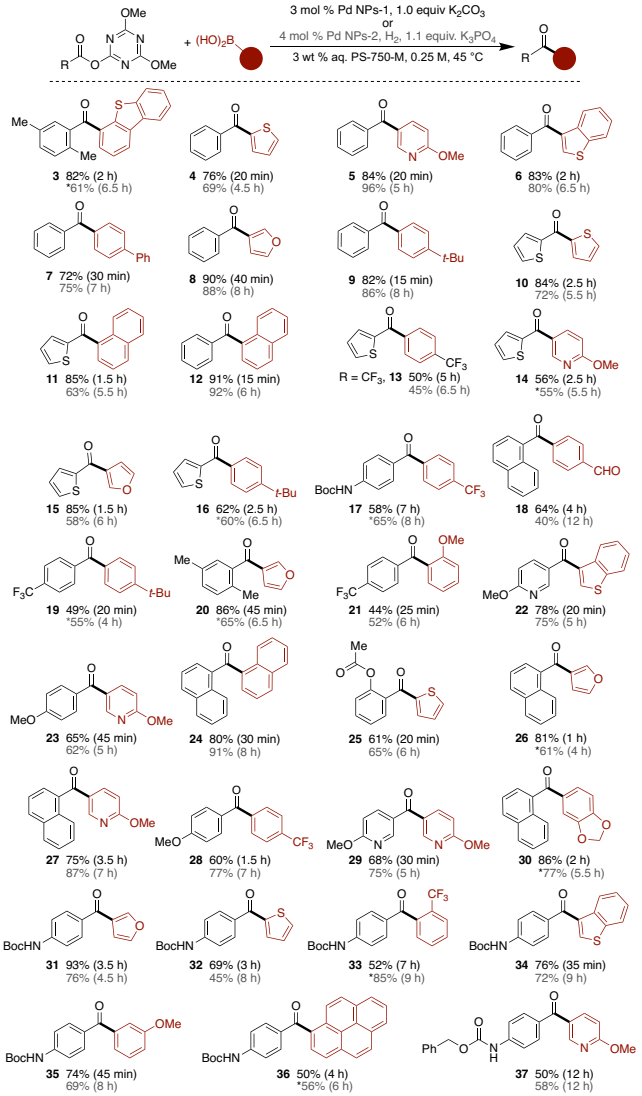

[a]**Conditions:** Triazine ester (0.25 mmol), (hetero)arylboronic acid (0.375 mmol), catalyst (3 mol % **NPs-1** or 4 mol % **NPs-2**) = **NPs** [**NPs-1** derived from $Pd_2(dba)_3$ and K_2CO_3 (0.25 mmol) or **NPs-2** derived from $Pd_2(dba)_3$, H_2, and K_3PO_4 (0.25 mmol)], 0.9 mL 3 wt % aq. PS-750-M, 0.1 mL THF, 45 °C. *Yields based on the average of two runs. All yields are isolated.

To find whether the catalyst is effective with the polarity reversal of coupling partners, we performed a reaction between benzoic acid adduct **38** and thiopheneboronic acid **39** using **NPs-1**

(Scheme 2A). In this case, 76% isolated yield of product **4** was obtained in 20 minutes of reaction time. Instead, when thiophenylcarboxylic acid adduct **40** and phenylboronic acid **41** were exposed under the same conditions, product **4** was obtained in a 62% isolated yield in 2 hours. Although the reaction rate was slow due to changes in electronics in nucleophile and electrophile, good reactivity was observed.

Next, the scalability of this catalytic methodology was evaluated on a gram-scale reaction between carboxylic acid adduct **42** and boronic acid **43** (Scheme 2B). In this reaction, product **34** was obtained in 92% isolated yield, 13% more yield than the one obtained on a 0.25 mmol scale reaction. Therefore, this methodology is scalable and works better on large-scale reactions.

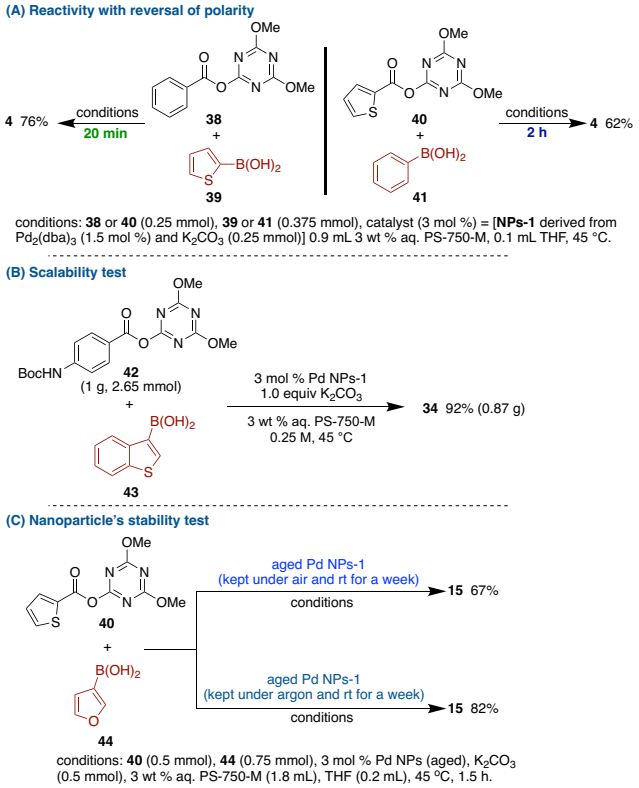

Scheme 2. Activity tests of nanoparticles. (A) Reactivity test with reversal of polarity. (B) Gram-scale reaction using **NPs-1**. (C) Stability of **NPs-1** under argon and air atmosphere.

NPs stability was also accessed under argon and air atmospheres at room temperature (rt). The **NPs-1** kept under argon atmosphere at rt for a week were equally efficient as freshly or in-situ prepared (Scheme 2C). A reaction of carboxylic acid adduct **40** and boronic acid **44** affords product **15** in 82% isolated yield, a similar yield obtained with a fresh catalyst. However, the catalyst became slightly less efficient when stored under air for a week, and a 67% isolated yield of product **15** was obtained.

To evaluate any induction time, we compared the % yield of **3** at different time intervals using **NPs-1**, **NPs-2**, and **NPs-3** (Scheme 3). Notably, the latter was cautiously prepared by the addition of Grignard reagent to the Pd source and capping the resulting particles with aq. PS-750-M (for details, see Supporting Information, page S8). In the reaction between **1** and **2**, the trends in reaction rate were similar with the **NPs-1** and **NPs-3**, although the reaction was slightly slower when **NPs-3** were used. In contrast, **NPs-2** were significantly less efficient and provided a 48% yield of **3** in 2 hours, while with **NPs-1**, product **3** was obtained in an 82% yield. In this case, $t_{1/2}$ was only 48 minutes compared to > 2 h with **NPs-2** and > 1 h with **NPs-3**. Therefore, the naturally formed Pd(0) NPs bound to PS-750-M molecules are more efficient than other types of NPs.

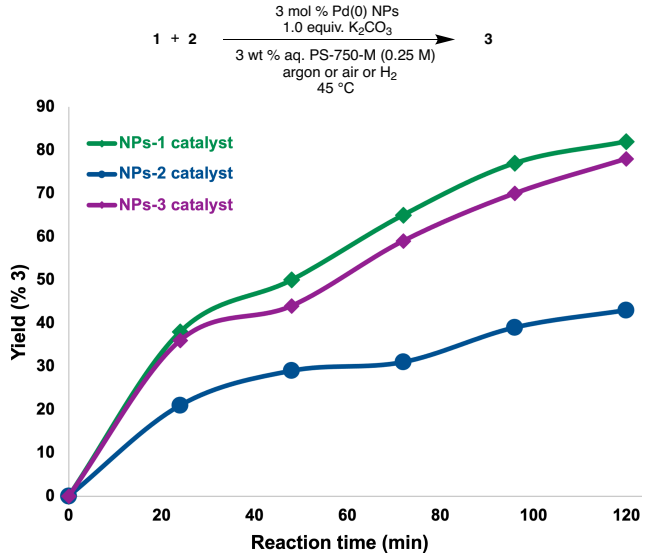

Scheme 3. Reaction profile using different nanoparticles.

CONCLUSION. In summary, the water-sensitive triazine adducts of carboxylic acids can efficiently afford non-symmetric ketones in water via cross-couplings with boronic acids using naturally formed Pd(0) NPs from the air- and water-sensitive Pd_2dba_3 as NPs precursor. These NPs are much more effective than those requiring any reductant for their formation, and reaction rates were faster for a broad range of substrates. The shielding effect of micelles stabilizes both the NPs and triazine adduct to enable the catalysis efficiently. Both the NPs and catalytic reaction are scalable and sustainable. The methodology is safer because it does not involve any reductant and toxic organic solvent. Since no phosphine ligands are involved in catalysis, this methodology is affordable.

MATERIALS AND METHODS.

All manipulations were carried out under argon atmosphere unless otherwise noted. Solvent molarity listed in reaction schemes is relative to the limiting reagent.

Chromatography. TLC plates (UV 254 indicator, aluminum backed, 175-225 µm thickness, standard grade silica gel, 230–400 mesh) was supplied by Merck; silica gel (60 Å pore size, 230-400 mesh) was purchased from Silicycle; sand was purchased from Fisher Chemical and VWR scientific.

Solvents. Ethyl acetate, hexanes, THF, and HPLC-grade water were purchased from Fisher Chemicals or MilliporeSigma. NMR solvents were obtained from MilliporeSigma; surfactant PS-750-M was prepared using the standard procedure and 3 wt % solution was prepared in HPLC-grade water. Poly(ethylene glycol) methyl ether 750 (mPEG-750-M) was supplied by Alfa-Aesar and MilliporeSigma.

Reagents. $Pd_2(dba)_3$ was supplied by MilliporeSigma. Arylboronic acids were purchased from MilliporeSigma or Combi-Blocks or Matrix Scientific. Commercially available carboxylic acids were either supplied by MilliporeSigma or Combi-Blocks

Inc. or Acros Organics or Alfa-Aesar. K_2CO_3 was purchased from MilliporeSigma.

General Instrumentation. All products were purified by manual column chromatography using silica gel (60 Å pore size, 230-400 mesh). NMR spectra were recorded at 23 °C on Varian MR-400 and Varian Unity INOVA 500 (400, 500, 700 MHz, respectively). Reported chemical shifts are referenced to residual solvent peaks. HRMS analyses were obtained either using a 5975C Mass Selective Detector coupled with a 7890A Gas Chromatograph (Agilent Technologies) or orbit-trap.

Optimized procedure for the synthesis of diaryl ketones using Pd NPs-1. 4.0 mL reaction vial containing a PTFE-coated magnetic stir bar was charged with triazine ester (0.50 mmol), Pd_2dba_3 (1.5 mol %, equivalent to 3 mol % Pd NPs), K_2CO_3 (0.50 mmol), and appropriate arylboronic acid (0.75 mmol). Later, freshly argon purged 1.8 mL 3 wt % aq. PS-750-M and 0.2 mL THF were added, and the reaction vial was closed with a rubber septum. The mixture was evacuated and backfilled with argon. The vial was transferred to a pre-heated stir plate at 45 °C and the mixture was stirred under argon atmosphere. After complete consumption of triazine ester as monitored by TLC, the reaction vial was opened, and 1-2 mL ethyl acetate was added. The mixture was then gently stirred for 2 min at rt. Stirring was stopped and the organic layer was separated using a pipette. This extraction procedure was repeated for an additional time. The combined organic layers were dried over anhydrous Na_2SO_4. Volatiles were removed under reduced pressure to obtain crude product, which was then purified by column chromatography over silica gel using hexanes/ethyl acetate as eluent.

Optimized procedure for the synthesis of diaryl ketones using Pd NPs-2. 4.0 mL reaction vial containing a PTFE-coated magnetic stir bar was charged with triazine ester (0.50 mmol), Pd_2dba_3 (2 mol %, equivalent to 4 mol % of NPs-2), K_3PO_4 (0.55 mmol), and appropriate arylboronic acid (0.75 mmol). Later, freshly argon purged 1.8 mL 3 wt % aq. PS-750-M and 0.2 mL THF were added, and the reaction vial was closed with a rubber septum. The mixture was evacuated and backfilled with argon. The vial was transferred to a pre-heated stir plate at 45 °C and the mixture was stirred under hydrogen atmosphere. After complete consumption of triazine ester as monitored by TLC, the reaction vial was opened, and 1-2 mL ethyl acetate was added. The mixture was then gently stirred for 2 min at rt. Stirring was stopped and the organic layer was separated using a pipette. This extraction procedure was repeated for an additional time. The combined organic layers were dried over anhydrous Na_2SO_4. Volatiles were removed under reduced pressure to obtain crude product, which was then purified by column chromatography over silica gel using hexanes/ethyl acetate as eluent.

ASSOCIATED CONTENT

Supporting Information

The Supporting Information is available free of charge on the ACS Publications website. Experimental procedures, compound characterization, spectroscopic data are included in this document (PDF).

AUTHOR INFORMATION

Corresponding Author

*sachin.handa@louisville.edu

Author Contributions

The manuscript was written through contributions of all authors. / All authors have given approval to the final version of the manuscript.

Funding Sources

This research was supported in part by the National Science Foundation under award number CHE-2044778.

Notes

The authors declare no competing financial interests.

ACKNOWLEDGMENT

We acknowledge Deborah S. Ogulu, Jagdeep Kaur Virdi, and Sudripet Sharma for technical assistance.

REFERENCES

(1) Kitanosono, T.; Masuda, K.; Xu, P.; Kobayashi, S. Catalytic Organic Reactions in Water toward Sustainable Society. *Chem. Rev.* **2018**, *118*, 679–746. https://doi.org/10.1021/acs.chemrev.7b00417

(2) Zhou, F.; Hearne, Z.; Li, C.-J. Water—the Greenest Solvent Overall. *Curr. Opin. Green Sustain. Chem.* **2019**, *18*, 118–123. https://doi.org/https://doi.org/10.1016/j.cogsc.2019.05.004

(3) Klijn, J. E.; Engberts, J. B. F. N. Fast Reactions 'on Water.' *Nature* **2005**, *435*, 746–747. https://doi.org/10.1038/435746a

(4) Romney, D. K.; Arnold, F. H.; Lipshutz, B. H.; Li, C.-J. Chemistry Takes a Bath: Reactions in Aqueous Media. *J. Org. Chem.* **2018**, *83*, 7319–7322. https://doi.org/10.1021/acs.joc.8b01412

(5) Lipshutz, B. H.; Ghorai, S.; Cortes-Clerget, M. The Hydrophobic Effect Applied to Organic Synthesis: Recent Synthetic Chemistry "in Water." *Chem. Eur. J.* **2018**, *24*, 6672–6695. https://doi.org/https://doi.org/10.1002/chem.201705499

(6) Cortes-Clerget, M.; Yu, J.; Kincaid, J. R. A.; Walde, P.; Gallou, F.; Lipshutz, B. H. Water as the Reaction Medium in Organic Chemistry: From Our Worst Enemy to Our Best Friend. *Chem. Sci.* **2021**, *12*, 4237–4266. https://doi.org/10.1039/D0SC06000C

(7) Ogulu, D.; Bora, P. P.; Bihani, M.; Sharma, S.; Ansari, T. N.; Wilson, A. J.; Jasinski, J. B.; Gallou, F.; Handa, S. Phosphine Ligand-Free Bimetallic Ni(0)Pd(0) Nanoparticles as a Catalyst for Facile, General, Sustainable, and Highly Selective 1,4-Reductions in Aqueous Micelles. *ACS Appl. Mater. Interfaces* **2022**, *14*, 6754–6761. https://doi.org/10.1021/acsami.1c22282

(8) Ansari, T. N.; Sharma, S.; Hazra, S.; Jasinski, J.; Wilson, A. J.; Hicks, F.; Leahy, D. K.; Handa, S. Shielding Effect of Nanomicelles: Stable and Catalytically Active Oxidizable Pd(0) Nanoparticle Catalyst Compatible for Cross-Couplings of Water-Sensitive Acid Chlorides in Water. *JACS Au,* **2021**, *1,* 1506. https://doi.org/10.1021/jacsau.1c00236

(9) Shi, P.; Zhang, H.; Lin, L.; Song, C.; Chen, Q.; Li, Z. Molecular Dynamics Simulation of Four Typical Surfactants in Aqueous Solution. *RSC Adv.* **2019**, *9*, 3224–3231. https://doi.org/10.1039/C8RA09670H.

(10) Zhang, Q.; Mao, Z.; Wang, K.; Phan, N. T. S.; Zhang, F. Microwave-Assisted Aqueous Carbon–Carbon Cross-Coupling Reactions of Aryl Chlorides Catalysed by Reduced Graphene Oxide Supported Palladium Nanoparticles. *Green Chem.* **2020**, *22*, 3239–3247. https://doi.org/10.1039/D0GC00833H.

(11) Wang, K.; Liu, J.; Zhang, F.; Zhang, Q.; Jiang, H.; Tong, M.; Xiao, Y.; Son Phan, N. T.; Zhang, F. Primary Amine-Functionalized Mesoporous Phenolic Resin-Supported Palladium Nanoparticles as an Effective and Stable Catalyst for Water-Medium Suzuki–Miyaura Coupling Reactions. *ACS Appl. Mater. Interfaces* **2019**, *11*, 41238–41244. https://doi.org/10.1021/acsami.9b11459.

(12) Friedman, D.; Masciangioli, T.; Olson, S. National Research Council (US) Chemical Sciences Roundtable. The Role of the Chemical Sciences in Finding Alternatives to Critical Resources: A Workshop Summary. National Academies Press (US); **2012**, p1-72. ISBN-13: 978-0-309-25429-8. https://www.ncbi.nlm.nih.gov/books/NBK97332/pdf/Bookshelf_NBK97332.pdf

(13) Martin, R.; Buchwald, S. L. Palladium-Catalyzed Suzuki−Miyaura Cross-Coupling Reactions Employing Dialkylbiaryl Phosphine Ligands. *Acc. Chem. Res.* **2008**, *41*, 1461–1473. https://doi.org/10.1021/ar800036s.

(14) Wang, Y.; Liu, Y.; Zhang, W.; Sun, H.; Zhang, K.; Jian, Y.; Gu, Q.; Zhang, G.; Li, J.; Gao, Z. Sustainable Ligand-Free, Palladium-Catalyzed Suzuki–Miyaura Reactions in Water: Insights into the Role of Base. *ChemSusChem* **2019**, *12*, 5265–5273. https://doi.org/https://doi.org/10.1002/cssc.201902853.

(15) Yamada, Y. M. A.; Yuyama, Y.; Sato, T.; Fujikawa, S.; Uozumi, Y. A Palladium-Nanoparticle and Silicon-Nanowire-Array Hybrid: A Platform for Catalytic Heterogeneous Reactions. *Angew. Chem., Int. Ed.* **2014**, *53*, 127–131. https://doi.org/https://doi.org/10.1002/anie.201308541.

(16) Handa, S.; Wang, Y.; Gallou, F.; Lipshutz, B. H. Sustainable Fe–Ppm Pd Nanoparticle Catalysis of Suzuki-Miyaura Cross-Couplings in Water. *Science* **2015**, *349*, 1087–1091. https://doi.org/10.1126/science.aac6936.

(17) Kaneko, H.; Matsumoto, T.; Cuya Huaman, J. L.; Ishijima, M.; Suzuki, K.; Miyamura, H.; Balachandran, J. Selection Criteria for Metal Precursors and Solvents for Targeted Synthesis of Metallic Nanostructures Via Kinetic Control in the Polyol Process. *Inorg. Chem.* **2021**, *60*, 3025–3036. https://doi.org/10.1021/acs.inorgchem.0c03266.

(18) Zalesskiy, S. S.; Ananikov, V. P. Pd2(Dba)3 as a Precursor of Soluble Metal Complexes and Nanoparticles: Determination of Palladium Active Species for Catalysis and Synthesis. *Organometallics* **2012**, *31*, 2302–2309. https://doi.org/10.1021/om201217r.

(19) Bringmann, G.; Gampe, C. M.; Reichert, Y.; Bruhn, T.; Faber, J. H.; Mikyna, M.; Reichert, M.; Leippe, M.; Brun, R.; Gelhaus, C. Synthesis and Pharmacological Evaluation of Fluorescent and Photoactivatable Analogues of Antiplasmodial Naphthylisoquinolines. *J. Med. Chem.* **2007**, *50*, 6104–6115. https://doi.org/10.1021/jm061464w.

(20) Taladriz, A.; Healy, A.; Flores Pérez, E. J.; Herrero García, V.; Ríos Martínez, C.; Alkhaldi, A. A. M.; Eze, A. A.; Kaiser, M.; de Koning, H. P.; Chana, A.; Dardonville, C. Synthesis and Structure–Activity Analysis of New Phosphonium Salts with Potent Activity against African Trypanosomes. *J. Med. Chem.* **2012**, *55*, 2606–2622. https://doi.org/10.1021/jm2014259.

(21) Wu, S.-B.; Long, C.; Kennelly, E. J. Structural Diversity and Bioactivities of Natural Benzophenones. *Nat. Prod. Rep.* **2014**, *31*, 1158–1174. https://doi.org/10.1039/C4NP00027G.

(22) Reitzenstein, D.; Quast, T.; Kanal, F.; Kullmann, M.; Ruetzel, S.; Hammer, M. S.; Deibel, C.; Dyakonov, V.; Brixner, T.; Lambert, C. Synthesis and Electron Transfer Characteristics of a Neutral, Low-Band-Gap, Mixed-Valence Polyradical. *Chem. Mater.* **2010**, *22*, 6641–6655. https://doi.org/10.1021/cm102650h.

(23) Blakeney, J. S.; Reid, R. C.; Le, G. T.; Fairlie, D. P. Nonpeptidic Ligands for Peptide-Activated G Protein-Coupled Receptors. *Chem. Rev.* **2007**, *107*, 2960–3041. https://doi.org/10.1021/cr050984g.

(24) Nohynek, G. J.; Schaefer, H. Benefit and Risk of Organic Ultraviolet Filters. *Regul. Toxicol. Pharmacol.* **2001**, *33*, 285–299. https://doi.org/https://doi.org/10.1006/rtph.2001.1476.

(25) Gao, Y.; Liu, J.; Li, Z.; Guo, T.; Xu, S.; Zhu, H.; Wei, F.; Chen, S.; Gebru, H.; Guo, K. Dichloroimidazolidinedione-Activated Beckmann Rearrangement of Ketoximes for Accessing Amides and Lactams. *J. Org. Chem.* **2018**, *83*, 2040–2049. https://doi.org/10.1021/acs.joc.7b02983.

(26) Kanta De, S. Vanadyl Triflate as an Efficient and Recyclable Catalyst for the Synthesis of A-Aminonitriles. *Synth. Commun.* **2005**, *35*, 1577–1582. https://doi.org/10.1081/SCC-200061547.

(27) Mokhtari, J.; Naimi-Jamal, M. R.; Hamzeali, H.; Dekamin, M. G.; Kaupp, G. Kneading Ball-Milling and Stoichiometric Melts for the Quantitative Derivatization of Carbonyl Compounds with Gas–Solid Recovery. *ChemSusChem* **2009**, *2*, 248–254. https://doi.org/https://doi.org/10.1002/cssc.200800258.

(28) Nakajima, M.; Fava, E.; Loescher, S.; Jiang, Z.; Rueping, M. Photoredox-Catalyzed Reductive Coupling of Aldehydes, Ketones, and Imines with Visible Light. *Angew. Chem., Int. Ed*. **2015**, *54*, 8828–8832. https://doi.org/https://doi.org/10.1002/anie.201501556.

(29) Gmouh, S.; Yang, H.; Vaultier, M. Activation of Bismuth(III) Derivatives in Ionic Liquids: Novel and Recyclable Catalytic Systems for Friedel−Crafts Acylation of Aromatic Compounds. *Org. Lett.* **2003**, *5*, 3365. https://doi.org/10.1021/ol030086b.

(30) Sartori, G.; Maggi, R. Use of Solid Catalysts in Friedel−Crafts Acylation Reactions. *Chem. Rev.* **2006**, *106*, 1077–1104. https://doi.org/10.1021/cr040695c.

(31) Wang, X.; Zhang, L.; Sun, X.; Xu, Y.; Krishnamurthy, D.; Senanayake, C. H. Addition of Grignard Reagents to Aryl Acid Chlorides: An Efficient Synthesis of Aryl Ketones. *Org. Lett.* **2005**, *7*, 5593–5595. https://doi.org/10.1021/ol052150q.

(32) Duplais, C.; Bures, F.; Sapountzis, I.; Korn, T. J.; Cahiez, G.; Knochel, P. An Efficient Synthesis of Diaryl Ketones by Iron-Catalyzed Arylation of Aroyl Cyanides. *Angew. Chem., Int. Ed.* **2004**, *43*, 2968–2970. https://doi.org/https://doi.org/10.1002/anie.200453696.

(33) Liu, K.-J.; Jiang, S.; Lu, L.-H.; Tang, L.-L.; Tang, S.-S.; Tang, H.-S.; Tang, Z.; He, W.-M.; Xu, X. Bis(Methoxypropyl) Ether-Promoted Oxidation of Aromatic Alcohols into Aromatic Carboxylic Acids and Aromatic Ketones with O2 under Metal- and Base-Free Conditions. *Green Chem.* **2018**, *20*, 3038–3043. https://doi.org/10.1039/C8GC00223A.

(34) Wu, X.-F.; Neumann, H.; Beller, M. Synthesis of Heterocycles via Palladium-Catalyzed Carbonylations. *Chem. Rev.* **2013**, *113*, 1–35. https://doi.org/10.1021/cr300100s.

(35) Heck, R. F. A Synthesis of Diaryl Ketones from Arylmercuric Salts. *J. Am. Chem. Soc.* **1968**, *90*, 5546–5548. https://doi.org/10.1021/ja01022a040.

(36) Rérat, A.; Michon, C.; Agbossou-Niedercorn, F.; Gosmini, C. Synthesis of Symmetrical Diaryl Ketones by Cobalt-Catalyzed Reaction of Arylzinc Reagents with Ethyl Chloroformate. *Eur. J. Org. Chem.,* **2016**, *26*, 4554–4560. https://doi.org/https://doi.org/10.1002/ejoc.201600738.

Table of Contents Graphic